

### Structural and Dielectric Investigations on Pure and Doped Triglycine Sulfate (TGS) Crystals

Adel Shaheen<sup>a</sup>, Mohammad Aljarrah<sup>b</sup>, Morad Etier<sup>b</sup>, Amjad H. El-Sheikh<sup>c</sup> and Fathy Salman<sup>d</sup>

<sup>a</sup> Department of Physics, Faculty of Science, The Hashemite University, P.O. Box 330127, Zarqa 13133, Jordan.

<sup>b</sup> Department of Industrial Engineering, Faculty of Engineering, The Hashemite University, P.O. Box 330127, Zarqa 13133, Jordan.

<sup>b</sup> Chemistry Department, Faculty of Science, The Hashemite University, P.O. Box 330127, Zarqa 13133, Jordan.

<sup>b</sup> Physics Department, Benha University, Benha, Egypt.

**Doi:** <https://doi.org/10.47011/15.4.5>

Received on: 15/01/2021;

Accepted on: 22/03/2021

---

**Abstract:** In this paper, a single crystal triglycine sulfate (TGS) doped with copper sulfate was synthesized using the slow evaporation technique. Structural characterization was carried out using X-ray diffraction and FTIR techniques. Thermal studies revealed that the addition of copper sulfate did not affect the thermal stability of the TGS. In addition, intensive dielectric investigation has been carried out, which showed that the addition of copper sulfate enhances the dielectric permittivity. A change in Curie temperature has been observed upon doping TGS with copper sulfate.

**Keywords:** TGS doping, Copper sulfate, Dielectrics, Cole-Cole plot.

## 1. Introduction

Triglycine sulfate (TGS) has good pyroelectric and ferroelectric properties at room temperature. The material is crucial in fabricating electromechanical transducers and infrared sensors [1–4]. Hoshino *et al.* [5] reported that TGS crystallizes with monoclinic structure at room temperature with space group P21. On the other hand, polarization of TGS disappears above its Curie temperature (320K), where the material undergoes second-order phase transition and its space group changes to P21/m.

Horiuchi *et al.* [6] and Rai *et al.* [7] reported that the Curie temperature of TGS is 322 and 323 K, respectively. The structure of TGS ((NH<sub>2</sub>CH<sub>2</sub>COOH)<sub>3</sub>.H<sub>2</sub>SO<sub>4</sub>) is composed from 2(N<sup>+</sup>H<sub>3</sub>CH<sub>2</sub>COOH), N<sup>+</sup>H<sub>3</sub>CH<sub>2</sub>COO<sup>-</sup> and tetrahedron SO<sub>4</sub><sup>-2</sup> that are held together with

hydrogen bonds [8]. When TGS is exposed to polarized water, the hydrogen bonds break and TGS dissolves into the aqueous phase [8]. Ćwikiel *et al.* [9] studied nuclear magnetic resonance (NMR) of TGS crystal and found a decrease in the dielectric properties after twelve hours of applying, a DC field on the TGS crystal.

Several studies [10–12] reported that undoped TGS crystals have disadvantages over doped ones, like the easiness of depolarization and the high mobility of ferroelectric domains. Dielectric properties of TGS are associated with its domain structure which plays an important role in the function of pyroelectric detectors [10–12].

Many researchers have studied the effect of different dopant materials to enhance the pyroelectric and ferroelectric properties of TGS crystals [13–20]. To the best of our knowledge, doping TGS with copper sulfate has not been done so far. The aim of the current work is to investigate the electric and dielectric properties of pure TGS and doped TGS with copper sulfate. Doped and undoped TGS crystals were prepared by using the solution method with slow evaporation.

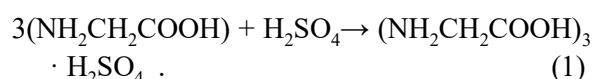
## 2. Experimental Work

### 2.1 Synthesis of Triglycine Sulphate (TGS) Crystals

The undoped TGS crystal and CuSO<sub>4</sub>-doped TGS crystal were grown by the slow evaporation technique in an aqueous solution. The slow evaporation method is a common one in preparing such materials, since it is an easy method and enough to obtain a single crystal material. Pure TGS salt was synthesized by mixing 75.07 g of analaR glycine ( $\geq 99.5\%$ ) with the formula of (NH<sub>2</sub>CH<sub>2</sub>COOH) and 17.7

mL concentrated sulphuric acid (H<sub>2</sub>SO<sub>4</sub>, 98%), which corresponds to the molar ratio 3:1. The mother solution was prepared by dissolving the synthesized salt of TGS in de-ionized water. After that, the mother solution was constantly stirred for two hours using a magnetic stirrer to obtain a homogenous solution.

Glycine reacts with sulphuric acid as follows [12, 21]:



This solution was filtered out to remove the undissolved particles. The filtered solution was covered with perforated sheet and kept for slow evaporation at room temperature for 28 days. Optically transparent crystals (Pure TGS) were obtained as shown in Fig. 1(a). 1 mol% of CuSO<sub>4</sub> was added to the pure TGS to prepare CuSO<sub>4</sub>-doped TGS. Although all growth parameters were kept the same as for pure TGS, transparent and good-quality crystals of CuSO<sub>4</sub>-doped TGS were achieved in approximately 15 days, as shown in Fig. 1(b).

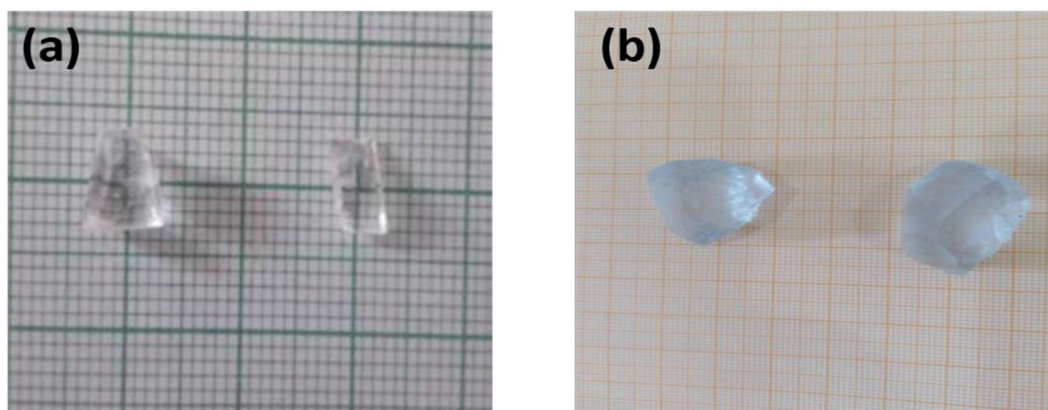


FIG. 1. The synthesized samples of (a) Un doped TGS crystal and (b) CuSO<sub>4</sub>-doped TGS crystal.

### 2.2 Characterization Techniques

The TGS single crystals were ground to powder form and then subjected to X-ray diffraction (XRD) with Cu-K $\alpha$  radiation ( $\lambda = 1.54056 \text{ \AA}$ ) [22]. The morphologies of the studied samples were characterized using scanning electron microscopy (SEM). Thermal history during heating and cooling was measured using differential scanning calorimetry (DSC). FTIR spectra were measured using a Vertex 70 FT-IR spectrometer (Bruker, Ltd., USA). Crystal samples for dielectric measurements were polished and their opposite faces were coated with high-grade silver paste

(this is to form two electrodes) to obtain a good conductive surface layer. The dielectric data was calculated in terms of the real and imaginary parts  $Z'$  and  $Z''$  of the impedance  $Z$  that was measured using a Solarton-1260 Impedance /Gain Phase analyzer in the frequency range of 1 Hz to 1MHz. The dielectric constant is calculated from [23]:

$$\epsilon' = \frac{C}{\epsilon_0} \times \frac{t}{A} = \frac{1}{\omega Z'' \epsilon_0} \times \frac{t}{A} \quad (2)$$

where  $C$  is the capacitance,  $t$  is the thickness of the sample ( $t=1\text{mm}$ ),  $\epsilon_0=8.854 \times 10^{-12} \text{ F/m}$  is the permittivity and  $A$  is the cross-sectional area of the sample (the radius of the sample was 0.5cm).

The dielectric loss ( $\tan \delta$ ) was calculated using the following equation [24-25]:

$$\tan \delta = \frac{z''}{z'}. \quad (3)$$

The dielectric loss ( $\epsilon''$ ) was calculated using the following equation [22]:

$$\epsilon'' = \epsilon' \tan \delta. \quad (4)$$

### 3. Results and Discussion

#### 3.1 XRD, SEM and DSC

The grown crystals have been characterized by powder X-ray diffractometer. Fig. 2(a,b) represents the powder X-ray pattern of the grown TGS. The system is found to exhibit a monoclinic structure with the space group P2

and the lattice parameters of pure TGS crystal are  $a=9.601 \text{ \AA}$ ,  $b=12.650 \text{ \AA}$  and  $c= 5.450 \text{ \AA}$ , which are in good agreement with the literature [7]. It is observed that doping of Cu in TGS crystals had no significant effect on XRD peak positions (i.e.,  $2\theta$  values), but the relative intensity of the peaks varied due to Cu doping, which may be due to the change in the electronic density in the crystallographic position of the TGS crystal. On the other hand, the X-ray diffraction shows identified peaks to the structure  $C_6H_{15}N_3O_6 \cdot H_2SO_4$  and other phases appeared related to the chalcantite  $CuSO_4 \cdot 5H_2O$ . Fig. 2(c) shows the SEM micrograph for the doped sample. A very smooth surface appeared in the graph without any evidence of cracks or impurities.

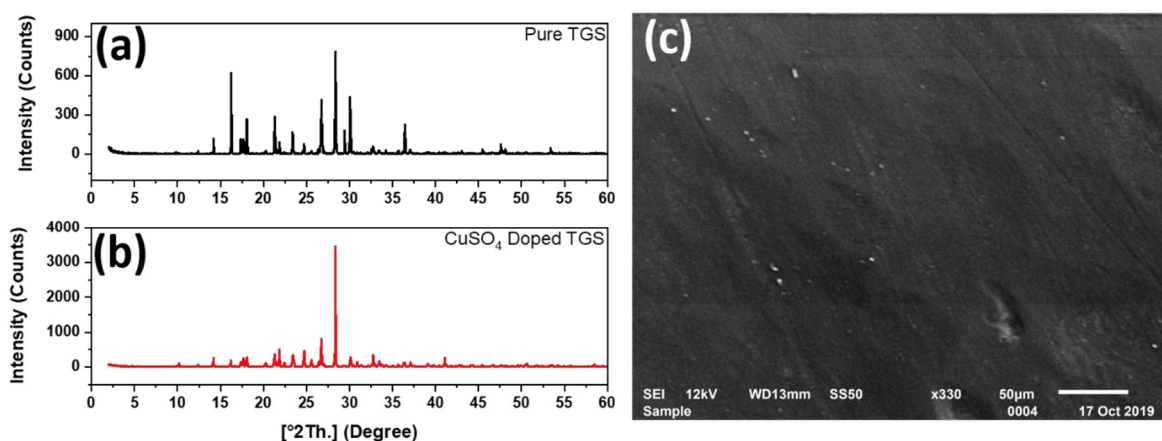


FIG. 2. X-ray diffraction pattern for (a) Pure TGS sample and (b)  $CuSO_4$  doped TGS crystal (c) Scanning electron microscopy surface for the  $CuSO_4$ -doped TGS crystal.

DSC analysis of pure TGS and  $CuSO_4$ -doped crystals is shown in Fig. 3. The melting point of TGS during heating was  $230^\circ C$ , which is in accordance to that reported by Sinha *et. al* [21] and Mahendra *et al.* [24]. The melting temperature

of  $CuSO_4$ -doped TGS crystal was found to be  $230^\circ C$ . Therefore, doping TGS with  $CuSO_4$  does not indicate any change in the thermal stability of TGS.

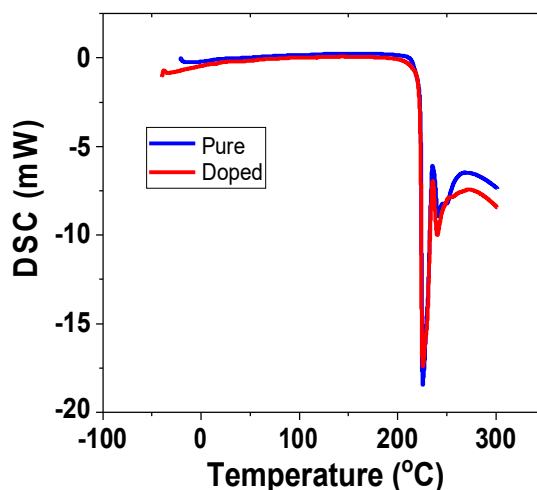


FIG. 3. DSC analysis for pure TGS and TGS doped with  $CuSO_4$  crystal.

The FTIR spectra were recorded for pure TGS and CuSO<sub>4</sub>-doped TGS within the wavenumber range 400-4000 cm<sup>-1</sup>. The spectra are shown in Fig. 4, while detailed assignments are given in Table 1. A comparison between our results and those previously reported in the literature [11, 21] was conducted in Table 1. Raja *et al.* (2017) [10] prepared an aluminum sulfate-doped TGS, while Sinha *et al.* (2015) [11] prepared a

crystal violet-doped TGS. It was noted that the characteristic IR absorption bands of pure TGS were very similar to those reported by Raja *et al.* (2017) [10]. They stated that doping TGS with aluminum sulfate did not affect the IR absorption bands for doping levels up to 1 mol%. A similar conclusion was obtained in this work where the doping of TGS with CuSO<sub>4</sub> did not significantly influence the IR absorption bands.

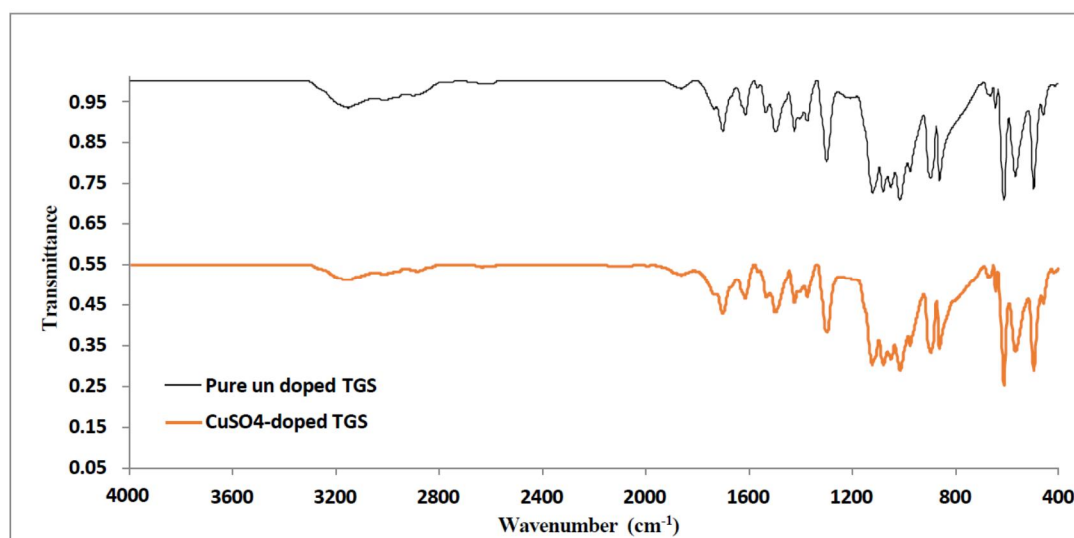


FIG. 4. Overlaid FTIR spectra of pure TGS crystal and CuSO<sub>4</sub>-doped TGS crystal.

TABLE 1. FTIR vibrational absorption bands (cm<sup>-1</sup>) of pure and CuSO<sub>4</sub>-doped TGS, their assignments and comparison with previous works.

Present work (pure and CuSO <sub>4</sub> -doped TGS)		Comparison with aluminum sulfate-doped TGS [11]		Comparison with crystal violet-doped TGS [21]	
Pure TGS	CuSO <sub>4</sub> -doped TGS	Band (cm <sup>-1</sup> )	Assignment	Band (cm <sup>-1</sup> )	Assignment
Broad band (2800-3350) with distinguished bands at 3154, 3020, 3007, 2961, 2901	Broad band (2800-3350) with distinguished bands at 3156, 3008, 2882			2800-3350	Asymmetric and symmetric N-H stretching of NH <sup>+</sup> <sub>3</sub> , C-H stretching of CH <sub>2</sub> , O-H stretching of H-bonded COOH
2637	2632	2638	CH <sub>2</sub> stretching		
1865	1861	1859	NH <sup>+</sup> <sub>3</sub> asymmetric bending		
1702	1702	1712	Overtones and combinations	1706	C=O stretching
1615	1615	1627	C=O stretching of COOH	1567-1623	Antisymmetric and symmetric stretching of COO <sup>-</sup>
1567	1565				
1536	1533			1501-1538	Bending vibrations of NH <sup>+</sup> <sub>3</sub>
1499	1497	1496	+ NH <sub>3</sub> asymmetric bending		
1425	1425	1419	NH <sup>+</sup> <sub>3</sub> asymmetric bending		

Present work (pure and CuSO <sub>4</sub> -doped TGS)		Comparison with aluminum sulfate-doped TGS [11]		Comparison with crystal violet-doped TGS [21]	
Pure TGS	CuSO <sub>4</sub> -doped TGS	Band (cm <sup>-1</sup> )	Assignment	Band (cm <sup>-1</sup> )	Assignment
1300	1298	1303	Asymmetric S=O stretching / CO <sub>2</sub> symmetric stretching + CH <sub>2</sub> twisting		
1122	1123	1126	NC <sup>α</sup> <sub>2</sub> stretching + NC <sup>α</sup> <sub>3</sub> stretching	977-1127	2-SO <sub>4</sub>
1081	1080				
1016	1015	1018	SO <sub>4</sub> vibrations		
976	976				
897, 863	896, 863	902, 856	C-C stretching		
613	613			501-615	NH <sup>+</sup> 3 oscillations
569	568	570	NH <sup>+</sup> torsional oscillations 3		
498	498	501	NH <sup>+</sup> oscillation 3		

The broad band between 2800 and 3350 cm<sup>-1</sup> in the spectra indicates asymmetric and symmetric N-H stretching of NH<sub>3</sub><sup>+</sup>, C-H stretching of CH<sub>2</sub>, O-H stretching of H-bonded COOH. Multiple combinations and overtone bands of CH<sub>2</sub> have been observed in the region 2300-2650 cm<sup>-1</sup>. The C=O stretching of carbonyl groups displayed its characteristic peak around 1712 cm<sup>-1</sup>.

The absorption in the region 1750-1550 cm<sup>-1</sup> is assigned to antisymmetric and symmetric stretching of C=O in COOH group. The peaks between 1530 and 1300 cm<sup>-1</sup> in the FTIR spectra can be assigned to NH<sub>3</sub><sup>+</sup> asymmetric bending, asymmetric S=O stretching, CO<sub>2</sub> symmetric stretching and CH<sub>2</sub> twisting. The CH<sub>2</sub> bending modes of glycine are located at 1300 cm<sup>-1</sup> and 1425 cm<sup>-1</sup>. The NH<sub>3</sub><sup>+</sup> displays its characteristic bending modes at 1425, 1499 and 1536 cm<sup>-1</sup>. The peak position between 950 and 1080 cm<sup>-1</sup> is assigned to stretching modes of carboxyl and sulfate ions.

The peaks due to NH<sub>3</sub><sup>+</sup> oscillations are seen at 896, 569 and 498 cm<sup>-1</sup>. The assignments showed that the hydrogen bonding extends throughout the TGS mixed CuSO<sub>4</sub> molecules. Some of the bands of the copper sulfate-doped TGS samples are either broadened or narrowed, which indicates the presence of copper sulfate in the doped TGS crystal.

### 3.2 Temperature Dependence of Dielectric Constant $\epsilon'$ and Dielectric Loss $\epsilon''$

The dielectric constant of the TGS crystals was calculated as a function of temperature at different frequencies, as shown in Fig. 5(a). The magnitude of the dielectric constant increases with temperature till 53°C (Curie temperature), then it decreases for all studied frequencies. The decrease in the dielectric constant above Curie temperature is in accordance with Weiss law [13]. The rapid increase of the dielectric constant may be due to space-charge polarization of thermally generated carriers and the existence of impurities in the TGS lattice [26]. Moreover, the increase of the dielectric constant with temperature – at a certain frequency – as shown in Fig. 5(a) is due to the contribution from the four types of polarizations (i.e., orientation, electronic, ionic and space charge). The decrease in the dielectric constant when the temperature is increased (Fig. 6) may be due to that the orientation polarization varies inversely with temperature [27] or because of the relaxation time which has been found to be fast at high temperatures and increases dramatically at low temperatures, suggesting a freezing of electric dipoles at low temperatures [28]. The temperature dependence dielectric loss of TGS crystals is shown in Fig. 5(b). It can be noticed that temperature has no significant effect on the dielectric loss.

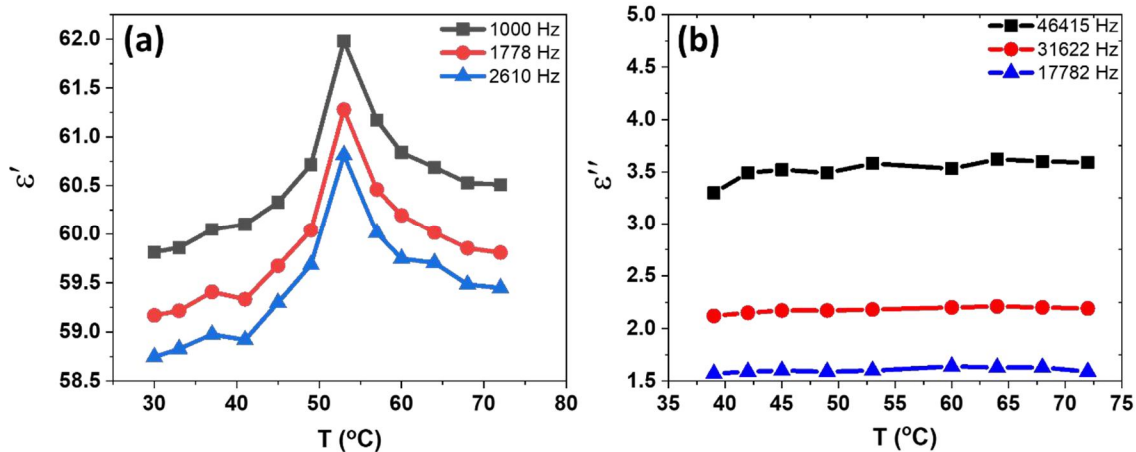


FIG. 5. Frequency dependence of (a) dielectric constant  $\epsilon'$  and (b) dielectric loss  $\epsilon''$  for pure TGS sample.

The obtained results of frequency dependencies of the real  $\epsilon'$  and the imaginary  $\epsilon''$  parts of the complex dielectric permittivity in single crystal TGS at different temperatures are shown in Fig. 6. The values of both the real  $\epsilon'$  and the imaginary  $\epsilon''$  parts are monotonically decreased with increasing frequency. The decrease in the dielectric constant as the frequency increases (Fig. 6) is due to the fact

at higher frequency, only ionic and electronic polarizations contribute. The loss factor, on the other hand, has a small value at low frequency and increases to reach its maximum value as the frequency increases (see Fig. 6). This behavior exhibited by the loss factor may be due to the contributions from all the four types of polarization [29-30].

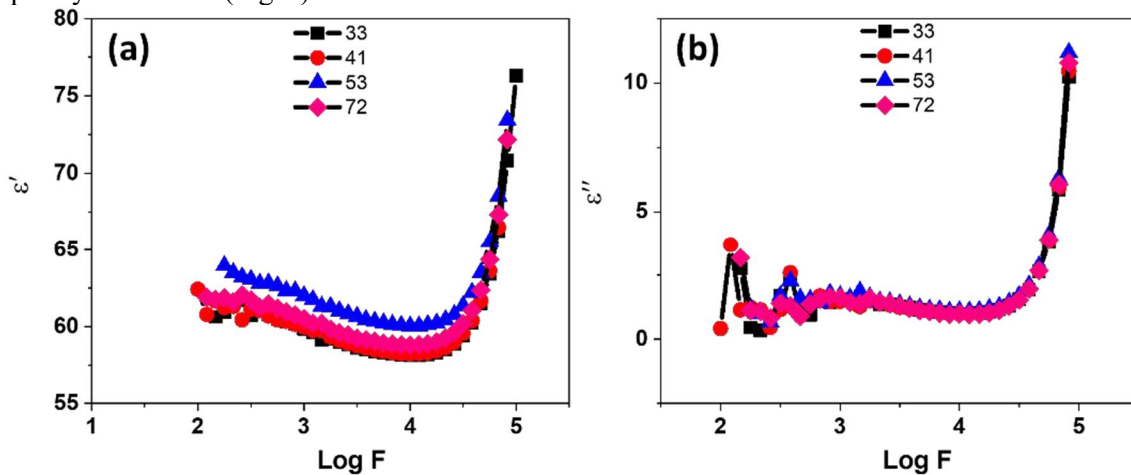


FIG. 6. Dielectric constant  $\epsilon'$  and dielectric loss  $\epsilon''$  versus  $\log f$  for the pure TGS sample.

### 3.3 Effect of $\text{CuSO}_4$ Doping

Variation of dielectric permittivity as a function of temperature (30-75°C) for both pure TGS and  $\text{CuSO}_4$ -doped TGS samples is shown in Fig. 7. The Curie temperatures for the pure sample and the doped one were observed to be 53°C and 55 °C, respectively. The dielectric constant increases up to the Curie temperature and then decreases obeying Curie-Weiss law

[13]. Adding  $\text{CuSO}_4$  caused an increase in the dielectric permittivity. The incorporation of  $\text{CuSO}_4$  in the structure can force the domains to fitter, which increases the value of permittivity [26]. Also, it is known that a multi-domain structure (e.g  $\text{CuSO}_4$ -doped TGS) exhibits higher spontaneous polarizing and dielectric constant than a single-domain structure.

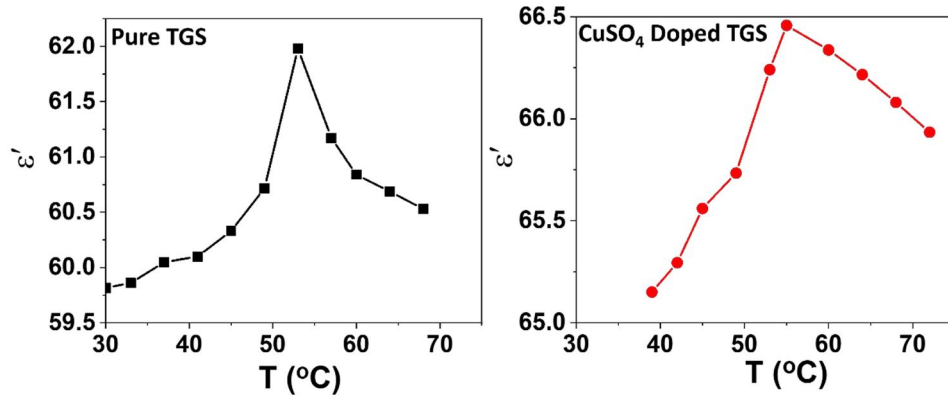


FIG. 7. Temperature dependence of dielectric permittivity of the pure and the doped TGS samples at  $f=1$  kHz.

### 3.4 COLE- COLE Plots

The Cole–Cole diagrams for TGS crystal at different temperatures in the frequency range (1kHz-1MHz) are shown in Fig. 8. Each plot appeared as a semicircle arc, intersecting the real axis at the values of  $\epsilon_\infty$  and  $\epsilon_S$  with its center being a part below the real axis and a straight line in the lower-frequency region. The values of  $\epsilon_S$ ,  $\epsilon_\infty$ ,  $\alpha$  and  $\tau$  were determined at different temperatures by a fitting circuit and are shown in Table (2). These values for pure TGS crystal

were found to be similar to those of doped TGS crystal.

Relaxation time  $\tau$  is a measure of the mobility of the molecules (dipoles) that exist in a material. The movement of dipoles under the field causes collisions and hence internal friction, so that the molecules turn slowly until reaching the final state of orientation polarization with relaxation time constant  $\tau$ . The obtained values of  $\tau$  calculated from fitting parameters, in general, are attenuated with increasing temperature.

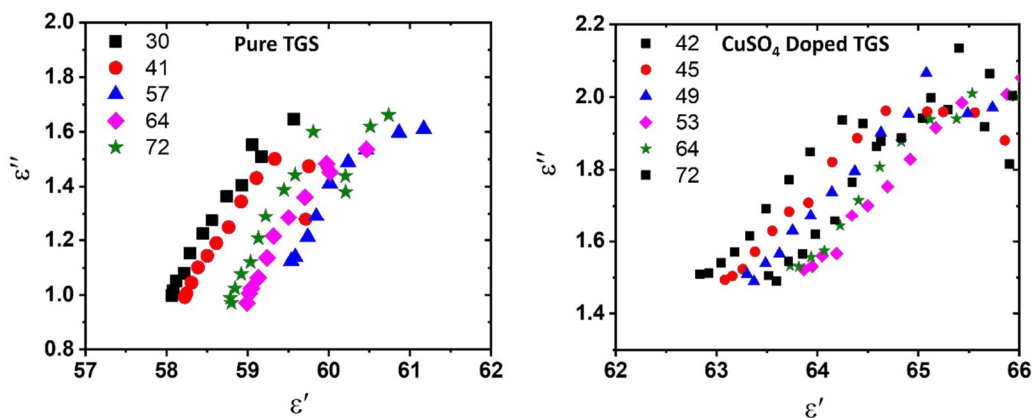


FIG. 8. The Cole-Cole plots for pure TGS and doped TGS samples at different temperatures.

TABLE 2. Infinite and static dielectric permittivity and relaxation time.

T (°C)	$\epsilon_\infty$	$\epsilon_S$	$\tau$
30	55.97	66.281	3.31E-06
33	56.655	69.516	2.16E-06
37	57.588	61.382	4.15E-05
41	57.427	61.878	0.000119
45	57.259	66.615	8.95E-05
49	57.67	66.187	8.95E-05
53	58.833	66.772	0.000256
57	58.041	65.433	0.000131
60	58.314	63.52	0.000181
64	58.345	62.396	0.000121
68	58.071	62.94	0.000159
72	58.018	64.416	8.95E-05

## 4. Conclusions

In this paper, TGS single crystal was successfully doped with copper sulfate. Doping TGS is still an area of interest due to the interesting output properties. It was observed that the addition of copper sulfate changes the Curie temperature of the TGS and an enhancement in dielectric permittivity was also

observed. The dielectric constant increased up to the Curie temperature and then decreased, thus Curie-Weiss law was obeyed. Moreover, the Cole–Cole diagrams for doped and un-doped TGS crystals at different temperatures in the frequency range (1kHz-1MHz) showed similar behaviors.

## References

- [1] Hang, T., Zhang, W., Ye, H.-Y. and Xiong, R.-G., *Chemical Society Reviews*, 40 (7) (2011) 3577.
- [2] Trybus, M., Proszak, W. and Woś, B., *Infrared Physics and Technology*, 54 (4) (2011) 326.
- [3] Novotný, J., Podvalová, Z. and Zelinka, J., *Crystal Growth and Design*, 3 (3) (2003) 393.
- [4] Sessler, G.M., *The Journal of the Acoustical Society of America*, 70 (6) (1981) 1596.
- [5] Hoshino, S., Okaya, Y. and Pepinsky, R., *Physical Review*, 115 (1959) 323.
- [6] Horiuchi, S. and Tokura, Y., *Nature Materials*, 7 (5) (2008) 357.
- [7] Rai, C., Byrappa, K. and Dharmaprasanth, S.M., *Physica B: Condensed Matter*, 406 (17) (2011) 3308.
- [8] Balakumar, S. and Zeng, H.C., *Journal of Materials Chemistry*, 10 (3) (2000) 651.
- [9] Ćwikiel, K., Medycki, W. and Stankowski, J., *Solid State Nuclear Magnetic Resonance*, 25 (1-3) (2004) 125.
- [10] Whatmore, R.W., *Reports on Progress in Physics*, 49 (12) (1986) 1335.
- [11] Raja, R., Santhanam, V., Vedhavalli, D. and Nathan, P.K., *International Journal of Materials Science*, 12 (2) (2017) 185.
- [12] Shanthi, N.T., Selvarajan, P. and Mahadevan, C.K., *Current Applied Physics*, 9 (5) (2009) 1155.
- [13] Bye, K.L., Whipps, P.W. and Keve, E.T., *Ferroelectrics*, 4 (1972) 253.
- [14] Lal, R.B. and Batra, A.K., *Ferroelectrics*, 142 (1993) 51.
- [15] Aravazhi, S., Jeyavel, R. and Subramanian, C., *Ferroelectrics*, 200 (1997) 390.
- [16] Gaffar, M.A. and Al-Fadl, A.A., *Cryst. Res. Technol.*, 34 (7) (1999) 915.
- [17] Sun, D., Yu, X. and Gu, Q., *Cryst. Res. Technol.*, 34 (10) (1999) 1255.
- [18] Su, G., He, Y., Yao, H., Shi, Z. and Eu, Q., *J. Cryst. Growth*, 209 (2000) 20.
- [19] Biedzycki, K., *Solid State Commun.*, 118, (2001) 141.
- [20] Alexandru, H.V., Berbecaru, C., Stanculescu, F. Pintile, L., Matei, I. and Lisca, M., *Sensors and Actuators A*, 113 (2004) 387.
- [21] Sinha, N., Bhandari, S., Yadav, H., Ray, G., Godara, S., Tyagi, N., Dalal, J., Kumar, S. and Kumar, B., *Cryst. Eng. Comm.*, 17 (2015) 5757.
- [22] Ayesha, A.I., Abu Haija, M., Shaheen, A. and Banat, F., *Applied Physics A*, 123 (2017) 682.
- [23] Alkhalzali, A., Etier, M., Aljarrah, M., Alsukker, A. and Salman, F., *World Journal of Engineering*, 16 (4) (2019) 477.
- [24] Ragahvan, C.M., Sankar, R., Mohankumar, R. and Jayavel, R., *Mater. Res. Bull.*, 43 (2008) 305.
- [25] Shaheen, A., Abu Haija, M., Chamakh, M., Assayed, G.A.I., Banat, F. and Ayesha, A.I., *Journal of Applied Polymer Science*, 137 (24) (2019) 48821
- [26] Mahendra, K., Kumar, H.K.T. and Udayashankar, N.K., *Appl. Phys. A*, 125 (2019) 228.
- [27] Banan, M., Lal, R.B. and Batra, A., *Journal of Materials Science*, 27 (1992) 2291.
- [28] Gregory, A.P. and Clarke, R.N., *NPL Report MAT*, (2012) 23.
- [29] Salman, F., Khalil, R. and Hazaa, H., *Adv. J. Phys. Sc.*, 3 (1) (2014) 1.
- [30] Maheshwari, P., "Electronic components and processes", (New Age International Publishers, 2008), p. 60.
- [31] Ahmad, M.M. and Yamada, K., *Appl. Phys. Lett.*, 19 (5) (2007) 052912-13.